III-1

Accelerators and Instruments

BL1U

Reconstruction of Free-Electron-Laser Optical Resonator at BL1U

H. Zen[1], J. Yamazaki[2], M. Fujimoto[2, 3], M. Hosaka[4], K. Hayashi[2], M. Katoh[2, 3] and H. Ohgaki[1]

[1]*Institute of Advanced Energy, Kyoto University, Uji 611-0011, Japan*

[2]*UVSOR Synchrotron Facility, Institute for Molecular Science, Okazaki 444-8585, Japan*

[3]*School of Physical Sciences, The Graduate University for Advanced Studies (SOKENDAI), Okazaki 444-8585, Japan*

[4]*Nagoya University Synchrotron radiation Research center, Nagoya 464-8603, Japan*

An electron storage-ring-driven Free Electron Laser (FEL) had been developed at the straight section #5, of the UVSOR using an optical klystron and FEL optical resonator until 2009 [1]. The straight section #5 had been also used for developing new coherent light sources, such as the coherent synchrotron radiation, the coherent harmonic generation by combining the high energy electron beam circulating in the storage ring and the high-power femtosecond laser. In 2010, dedicated undulators with an electromagnet-based bunching section were installed in the straight section #1 of the UVSOR. Then the above activities have been moved from straight section #5 to #1.

In this work, we tried to reconstruct the FEL optical resonator at the straight section #1 and BL1U to restart the FEL which will be used for the generation of high intensity gamma-rays as same as the HIγS in Duke University [2].

The new layout of the FEL optical resonator mirrors (M1 and M2) and the optical klystron at the straight section #1 is depicted in Fig. 1. The optical klystron has been already installed in 2012. In this work, the optical resonator mirrors were installed in the beamline and some commissioning experiments of the optical resonator were carried out.

The photographs of the vacuum chamber of the optical resonator mirrors are shown in Fig. 2. The vacuum chambers are supported by large gimbal mounts equipped with a motorized actuator to control the angle of mirrors. The resonator mirrors with the diameter of 1 inch are installed in the vacuum chamber. The downstream side gimbal mount is placed on the linear stage which enables us to change the total cavity length.

The commissioning experiment was performed at the wavelength of 540 nm. As a result, we could store the undulator radiation lights inside the optical resonator and observed strong lights from the resonator mirror as shown in Fig. 3. This indicates that the optical cavity mirrors has good alignment in the transverse direction. In the next machine time, the length of the optical resonator will be optimized to achieve the lasing of UVSOR-FEL with this new configuration.

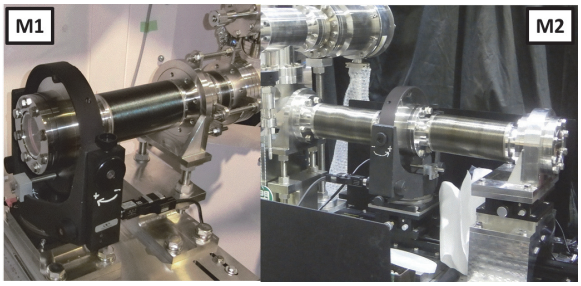

Fig. 2. Photograph of the vacuum chamber for FEL optical resonator mirrors.

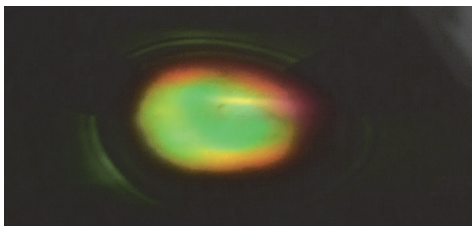

Fig. 3. Photograph of the strong lights from the optical resonator.

[1] H. Zen *et al*., Proc. of FEL2009 (2009) 576.
[2] http://www.tunl.duke.edu/web.tunl.2011a.higs.php

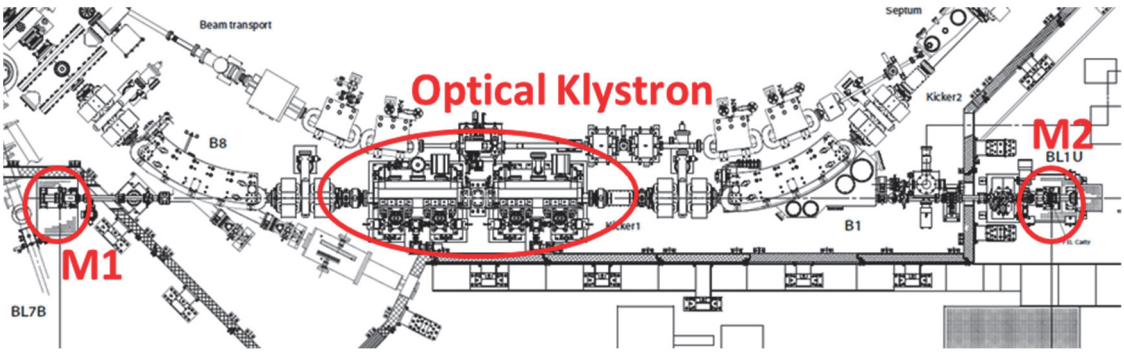

Fig. 1. Layout of FEL optical resonator mirrors (M1 and M2) and the optical klystron at the straight section #1 of UVSOR.

BL1U

Observation of XUV Vortex Beam from a Helical Undulator

T. Kaneyasu[1], Y. Hikosaka[2], M. Fujimoto[3, 4], H. Iwayama[3, 4], M. Hosaka[5], E. Shigemasa[3, 4] and M. Katoh[3, 4]

[1]*SAGA Light Source, Tosu 841-0005, Japan*
[2]*Graduate School of Medicine and Pharmaceutical Sciences, University of Toyama, Toyama 930-0194, Japan*
[3]*UVSOR Synchrotron Facility, Institute for Molecular Science, Okazaki 444-8585, Japan*
[4]*The Graduate University for Advanced Studies (SOKENDAI), Okazaki 444-8585, Japan*
[5]*Synchrotron Radiation Research Center, Nagoya University, Nagoya 464-8603, Japan*

An optical vortex beam carries orbital angular momentum (OAM), as well as spin angular momentum associated with its circular polarization. Recently it has been reported that the spiral motion of a relativistic electron naturally leads to the emission of photons carrying OAM [1]. A typical example of the vortex radiation is found in the harmonic radiation of a helical undulator in synchrotron light sources [2, 3]. Since the helical undulators are widely used in modern synchrotron light sources, the optical vortex beam generated as harmonic radiation may open up new opportunities in synchrotron radiation researches. Here we report on the observation of the extreme ultraviolet (XUV) vortex beam at 60 nm wavelength, produced as the second harmonic radiation from a helical undulator [4].

The experiment was carried out at the BL1U. To characterize experimentally the optical vortex beam, we observed an interference pattern between the photon beams from two helical undulators. The reference beam without OAM was produced as the fundamental radiation from the upstream undulator, while the optical vortex beam was produced as the second-harmonic radiation from the downstream undulator. The radiation wavelengths were set to 60 and 120 nm for the fundamental radiation from the upstream and downstream undulators, respectively. The spatial distribution of the photon beam was measured by scanning a pinhole.

Figure 1(a) compares the interference patterns measured for the left and right circular polarization modes. The direction of the spiral pattern changes with the helicity, as predicted in theoretical studies. The dotted curves in Fig. 1(b) show the calculated interference patterns, which agree with the experimental results. Thus, it is reasonable to conclude that optical vortex beams carrying an OAM of $l\hbar$ (l=±1) per photon are produced in the XUV region. In the present experiment, the electron beam emittance is 17.5 nm-radian, which is about four times larger than the 4.8 nm-radian corresponding to the diffraction-limited emittance at 60-nm wavelength Consequently, the measured spiral patterns are blurred, owing to the relatively large electron beam emittance, whereas an individual electron emits an optical vortex with a phase singularity and zero-intensity minimum. To reveal the overall features of the interference pattern smeared by the finite emittance, we performed a simulation using the SRW code [5] as in Fig. 1(c). It can be clearly seen that the simulation reproduces the experiments, which confirms the reliability of the measurement.

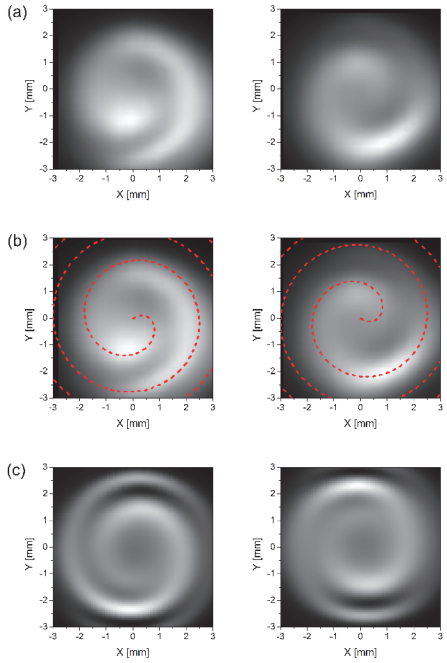

Fig. 1. Interference patterns at 60-nm wavelength produced by interfering the optical vortex beam with the reference beam without OAM. Left column: left circular polarization. Right column: right circular polarization. (a) Measurement results. (b) Same as (a) with the dotted curves representing the constructive interference patterns predicted by the theoretical model. (c) Simulation results by SRW code.

[1] M. Katoh et al., Sci. Rep. 7 (2017) 6130.
[2] S. Sasaki and I. McNulty, Phys. Rev. Lett. **100** (2008) 124801.
[3] J. Bahrdt et al., Phys. Rev. Lett. 111 (2013) 034801.
[4] T. Kaneyasu *et al.*, J. Synchrotron Rad. **24** (2017) 934.
[5] O. Chubar *et al.*, Nucl. Instrum. Meth. A **435** (1999) 495.

BL2A

Evaluation of a Flight High-Speed Back-Illuminated CMOS Sensor in a Soft X-Ray Range for FOXSI-3 Sounding Rocket Project

N. Narukage[1] and S. Ishikawa[2]

[1]*National Astronomical Observatory of Japan, Mitaka 181-8588, Japan*

[2]*Institute of Space and Astronautical Science, Japan Aerospace Exploration Agency, Sagamihara 252-5210, Japan*

The solar corona is full of dynamic phenomena. They are accompanied by interesting physical processes, namely, magnetic reconnection, particle acceleration, shocks, waves, flows, evaporation, heating, cooling, and so on. The understandings of these phenomena and processes have been progressing step-by-step with the evolution of the observation technology in EUV and X-rays from the space. But, there are fundamental questions remain unanswered, or haven't even addressed so far. Our scientific objective is to understand underlying physics of dynamic phenomena in the solar corona, covering some of the long-standing questions in solar physics such as particle acceleration in flares and coronal heating. In order to achieve these science objectives, we identify the imaging spectroscopy (the observations with spatial, temporal and energy resolutions) in the soft X-ray range (from ~0.5 keV to ~10 keV) is a powerful approach for the detection and analysis of energetic events [1]. This energy range contains many lines emitted from below 1 MK to beyond 10 MK plasmas plus continuum component that reflects the electron temperature.

The soft X-ray imaging spectroscopy is realized with the following method. We take images with a short enough exposure to detect only single X-ray photon in an isolated pixel area with a fine pixel Silicon sensor. So, we can measure the energy of the X-ray photons one by one with spatial and temporal resolutions. When we use a high-speed soft X-ray camera that can perform the continuous exposure with a rate of 1,000 times per second, we can count the photon energy with a rate of several 10 photons / pixel / second. This high-speed exposure is enough to track the time evolution of spectra generated by dynamic phenomena in the solar corona, whose lifetimes are about form several ten seconds to several minutes.

As the first imaging spectroscopic observation of the sun in soft X-ray range, we plan to launch the NASA's sounding rocket (FOXSI-3) in the summer of 2018.

In this time, we evaluated quantum efficiency (QE) of a flight back-illuminated high-speed CMOS sensor at UVSOR BL2A (see Fig. 1). The sensor was driven with a flight camera electronics board [2]. As a reference sensor, we used the photodiode AXUV100G. The preliminary result of the measured QE is shown in Fig. 2. The measured QE of the flight sensor is within the expected range that is calculated with the material and thickness of the sensor. Based on this QE measurement, we will finalize the thickness of the attenuation filter to adjust the incident X-ray flux into the sensor suitably for the photon counting.

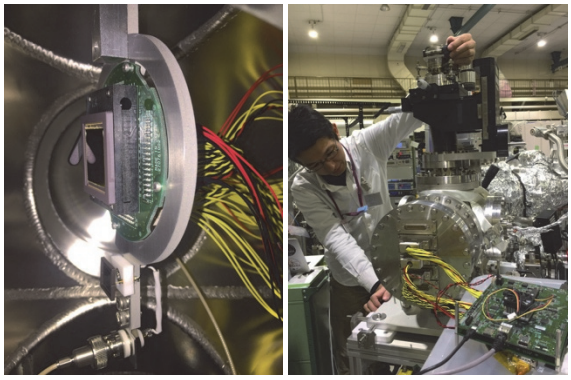

Fig. 1. Setting of CMOS sensor evaluation with a flight camera system. Left: CMOS sensor and photodiode deployed in a vacuum chamber. Right: Flight camera electronics board (green board in this picture).

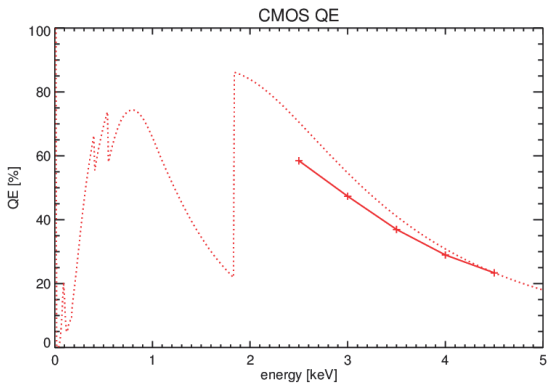

Fig. 2. Preliminary result of the measured quantum efficiency (QE) of the flight CMOS sensor. The solid and dotted lines show the measured and expected QE, respectively.

[1] N. Narukage *et al*., White paper of the "soft X-ray imaging spectroscopy", arXiv:1706.04536 (2017).
[2] S. Ishikawa *et al*., arXiv:1711.04372 (2017).

BL4U

Development of a Cryo-Cooling System for Scanning Transmission X-ray Microscopy

T. Ohigashi[1, 2], F. Kaneko[3], Y. Inagaki[1], T. Yano[1], H. Kishimoto[3] and N. Kosugi[1, 2]

[1]*UVSOR Synchrotron Facility, Institute for Molecular Science, Okazaki 444-8585, Japan*

[2]*School of Physical Sciences, SOKENDAI (The Graduate University for Advanced Studies), Okazaki 444-8585, Japan*

[3]*Sumitomo Rubber Industries, Kobe, 651-0072, Japan*

A scanning transmission X-ray Microscope (STXM) is a powerful tool to obtain 2-dimensional chemical states with high spatial resolution. By using the STXM in the soft X-ray region, core-level absorption edges of light elements, carbon, nitrogen and oxygen, are available for the measurement. Generally speaking, the radiation damage by X-rays is lower than that by electron beams [1]. This means that even organic materials, such as polymers, carbon nanotubes and biological specimens that are very sensitive to radiations, can be targets of the STXM. However, in spite of the lower radiation damage of X-rays, some samples show chemical or morphological changes during the measurement. For example, rubber, one of reasonable targets for the STXM analysis [2, 3], is easily damaged by the irradiation of X-rays. It is known that the cooling of rubber samples reduces radiation effects [4]. In the present work, therefore, we have developed a cryo-cooling system.

A Dewar vessel is placed on the STXM. Liquid nitrogen in the vessel cool a sample mounting plate through copper braids. A sample holder is equipped with two sets of a heater and a temperature sensor. One of these combinations is for the temperature control of samples and the other one is for keeping the temperature of stages constant. These heaters are operated by PID controllers. Main issues of the cryo-cooling system for STXM are the vibration generated by bubbling of liquid nitrogen and the thermal stability. In the present work, by optimizing thermal insulation and stiffness of the copper braids, the vibration at the sample is successfully reduced down to 50 nm (peak to valley). By using this system, the sample mounting plate can be cooled down to -90°C.

A thin specimen (thickness of 250 nm) of vulcanized rubber was used as a sample. After measuring an energy stack at nitrogen K-edge by changing dwell time as 1, 2 and 4 ms, the energy stack at carbon K-edge was measured to evaluate damages on the sample. NEXAFS spectra around carbon K-edge at RT and at cryo contion of -85°C and an STXM image of a damaged sample are shown in Fig. 1. In Fig. 1(a) and 1(b), main peaks are 285.4 and 288.0 eV, corresponded to C=C π* and C-H σ* transition respectively. The damage by X-ray irradiation mainly appears on 285.4 and 288.0 eV as decrease of intensity and as broadening of peak width. Especially, the peaks at 288.0 eV show apparent difference between RT and cryo conditions. In RT condition, peaks at 288.0 eV are dull and low rather than those in cryo condition although the lowest dose by the dwell time of 1 ms. Furthermore, height of the peaks at 285.4 in RT are lower than those in cryo condition. These differences show that using the cryo-cooling system is effective to reduce the damage on the sample. Currently, critical dose to analyze the vulcanized rubber and improvement of cryo temperature are under discussion.

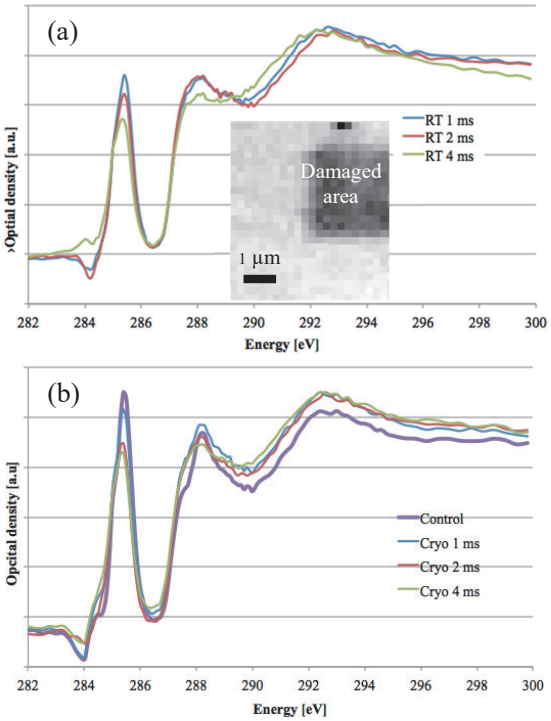

Fig. 1. NEXAFS spectra of pristine and damaged vulcanized rubber around carbon K-edge (a) at RT and (b) at -85°C. An inset in (a) is an STXM image of the damaged vulcanized rubber acquired at 285.4 eV.

[1] H. Ade *et al.*, Science 258 (1992) 972.
[2] D. A. Winesett *et al.*, Rubber. Chem. Technol. **76** (2003) 803.
[3] D. A. Winesett *et al.*, Rubber. Chem. Technol. **80** (2007) 14.
[4] G. Schneider, Ultramicroscopy **75** (1998) 85.

BL4U

High Pressure STXM Cell

P. –A. Glans[1], Y. S. Liu[1], R. M. Qiao[1], T. Ohigashi[2, 3] and J. –H. Guo[1]

[1]*Advanced Light Source, Lawrence Berkeley Nat'l Lab. 1 Cyclotron Road, Berkeley, CA 94720, USA*

[2]*UVSOR Synchrotron Facility, Institute for Molecular Science, Okazaki 444-8585, Japan*

[3]*School of Physical Sciences, The Graduate University for Advanced Studies (SOKENDAI), Okazaki 444-8585, Japan*

Measurements of the electronic structure of materials in vacuum or even at atmospheric pressure are becoming more and more common. Some catalytic reactions, however, occur at, or create, higher pressures: gas evolution (such as water splitting), some catalytic processes are more efficient at higher pressures, some batteries operate at pressures higher than 1 atm, High pressures are also necessary to investigate phase transitions of gasses.

A high-pressure cell for the STXM has been designed and tested at the BL4U at UVSOR, see Fig. 1. The body of the cell is made out of PEEK for maximum chemical compatibility. Windows similar to what is usually used at the STXM but with a custom window size were made at the Lawrence Berkeley Lab. The window size was 75μm x 75μm, set in frames of 5 mm x 5 mm and 10 mm x 10 mm. The cell was tested off-line and could reliably hold gauge pressures up to 10 bar. Liquid can flow through the cell through PEEK tubing. Once the system is filled, a valve on the drain end is closed and the system is pressurized by running the pump until required pressure has bee achieved.

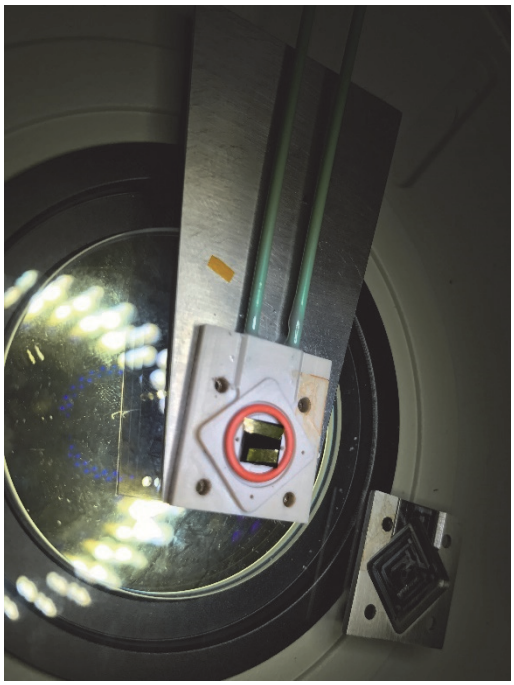

Fig. 1. Partially assembled high-pressure cell. The cell is mounted on the standard STXM sample holder.

The back window (5 mm x 5 mm frame) is visible together with Teflon spacers and the outer o-ring. A larger window (10 mm x 10 mm frame) will be mounted on top and the lid – visible to the right in the photo – will finish the 'sandwich.' The large window is rotated 45 degrees with respect to the smaller one.

The cell was loaded with water or $CaCl_2$ solutions with concentrations ranging from 0.5 M to 3.0 M. The pressure was controlled with a syringe pump and measured by a pressure gauge. In the STXM chamber we did not go past 2.0 bar gauge pressure for safety reasons. Figure 2 shows example data of the Ca $L_{2,3}$ edge XAS from 1.5 M solution of $CaCl_2$ in water at 0 bar gauge pressure and 2.0 bar gauge pressure.

The cell performed very well and we could collect spectra at elevated pressures. However, the next iteration needs a way to measure I0 and a solution to minimize the bulging of the windows. A future version of the cell will also include electrodes to allow for electrochemical reactions.

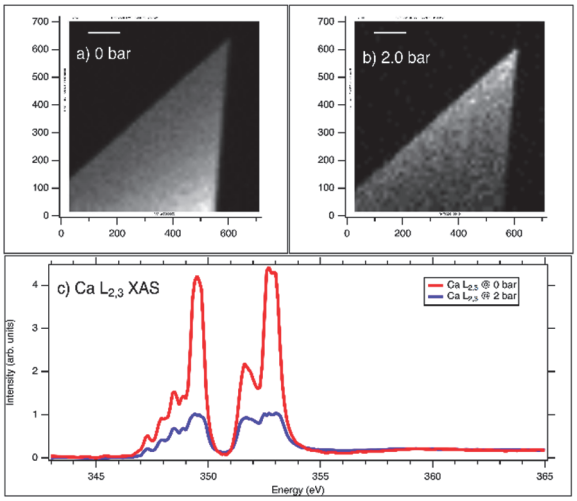

Fig. 2. STXM images of 1.5 M $CaCl_2$ solution at a) 0 bar gauge pressure, and at b) 2.0 bar gauge pressure. c) Cl $L_{2,3}$ XAS extracted from the images. Unfortunately, i) there was no access to an I_0 channel to normalize the spectra, and ii) the optical density was too high at higher pressures due to bulging cells so the XAS is saturated at 2.0 bar.

BL7B

Performance Verification of the VUV Coating for the CLASP2 Flight Mirrors

D. Song[1], R. Ishikawa[1], R. Kano[1], K. Shinoda[1] and M. Yoshida[2]
[1]*National Astronomical Observatory of Japan, Mitaka 181-8588, Japan*
[2]*Department of Astronomical Science, Graduate University for Advanced Studies (SOKENDAI), Tokyo 181-8585, Japan*

We are developing an ultraviolet spectro-polarimeter (SP) for a sounding rocket experiment named Chromospheric LAyer Spectro-Polarimeter (CLASP2). The CLASP2 is re-flight project of the Chromospheric Lyman-Alpha Spectro-Polarimeter (CLASP1), which successfully observed the Lyman-alpha polarization in 2015 [1], but will observe the polarization in 2019 with the different lines from the CLASP1 after a small modification in the optics. It mainly aims to achieve the high-sensitivity (< 0.1%) spectro-polarimetric observations in the Mg II h & k lines (near 280 nm) for deriving the magnetic information in the upper chromosphere of the Sun and also to get solar images in the Lyman-alpha line (121.6 nm) with the high temporal resolution. Therefore, it requires the high throughput not only near 280 nm but also around 121.6 nm wavelengths.

In this fiscal year, we prepared all CLASP2 flight mirrors. On the primary mirror of the telescope (TL), a dual-band pass "cold mirror" coating targeting both the 121.6 nm (R > 40%) and 280 nm (R > 70%) was performed by Acton Optics. In addition, the high reflectivity mirror coating (Al+MgF_2 coating) was done by Acton Optics on the new fabricated SP mirrors (R > 80% near 280 nm for convex hyperbolic mirrors and folder mirrors, and R > 75% near 121.6 nm for a slit mirror.

To evaluate their coating performance, we measured the reflectivity of witness samples (WSs) for the p- and s-polarized beam (hereafter, R_p and R_s) at the UVSOR BL7B. The WSs are 1-inch flat mirrors simultaneously coated with the flight mirrors during the coating processes [2]. For the primary mirror coating, WSs were spread over the area corresponding to the effective area of the primary mirror to check the uniformity of the reflectivity.

Figure 1 shows the reflectivity of the WSs for the primary mirror in the wide wavelength ranges. The measured reflectivity is larger than 55% near the 121.6 nm wavelength and also larger than 76% near the 280 nm wavelength. Meanwhile, the average reflectivity in the visible light wavelength ranges is less than 5%, which had been measured by the Acton Optics. This indicates that the "cold mirror" coating performed on the primary mirror not only has high reflectivity near our required UV wavelengths, but also efficiently eliminates unwanted lights such as visible light.

From Fig. 2, we can verify the performance of the high reflectivity coating at Angle of Incidence (AOI) as required by our SP mirrors. Note that, more information is given in Table 1.

Based on our measurements with WSs of the flight mirrors, we confirmed the following three: (1) The coatings performed on the flight mirrors (TL and SP) well satisfy our specifications. (2) The coating of the primary mirror (diameter: 290 m) is sufficiently uniform. (3) Finally, the computed throughput is about 1.8%, which is three times larger than the value of CLASP1 instrument (0.6%).

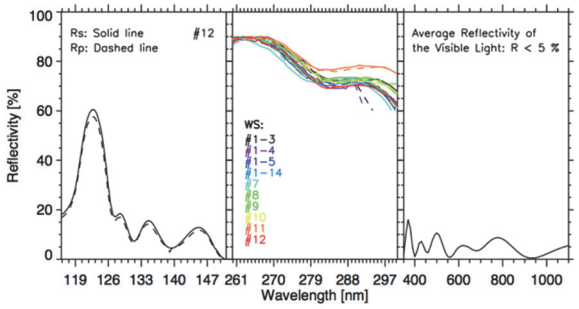

Fig. 1. Measured reflectivity of 10 witness samples for the primary mirror as a function of wavelengths.

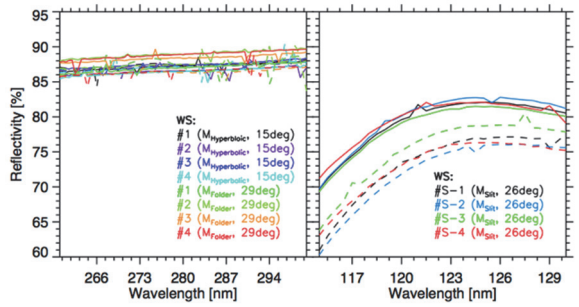

Fig. 2. Measured reflectivity of witness samples for the SP mirrors.

Table 1. Measured reflectivity of WSs for SP mirrors

Mirror	AOI (°)	R_p	R_s	$(R_p+R_s)/2$
$M_{Hyperbolic}$	11-18	87%	87.5%	87.3%
M_{Folder}	24-33	87%	88%	87.5%
M_{Slit}	22-30	73%	81%	77%

[1] R. Kano *et al.*, ApJL, **839** (2017), L10.
[2] N. Narukage *et al.*, UVSOR Activity Report **40** (2012) 46.

BL7B

Stokes Parameters Measurements of the BL7B by Using VUV Ellipsometry (III)

F. Sawa[1], S. Takashima[1], K. Fukui[1], K. Yamamoto[2], T. Saito[3] and T. Horigome[4]
[1]*Department of Electrical and Electronics Engineering, University of Fukui, Fukui 910-8507, Japan*
[2]*Far-infrared region Development Research Center, University of Fukui, Fukui 910-8507, Japan*
[3]*Department of Environment and Energy, Tohoku Institute of Technology, Sendai 982-8577, Japan*
[4]*UVSOR Synchrotron Facility, Institute for Molecular Science, Okazaki 444-8585, Japan*

Since it is difficult to construct vacuum ultraviolet region (VUV) ellipsometers, there exists only one beamline equipped with VUV spectroscopic ellipsometer (SE) at BESSY [1] in the world to our knowledge. Saito et al. proposed the other idea for VUV SE, which is dedicated to the synchrotron radiation (SR) and used an oblique incidence detector [2, 3]. Compared with the standard SE, this type of SE has an advantage in obtaining not only optical constants of the sample, but also Stokes parameters (S_1/S_0, S_2/S_0, S_3/S_0) (SPs) of the incident beam. We installed this type of SE at the BL7B of UVSOR. Since these SPs must be invariant even if the sample changes, we can use this characteristics as an indicator of the reliability of unknown sample experiment results. Therefore, we have been continuing to improve the reproducibility by eliminating the causes to reduce them. On the other hand, we have not confirmed the correctness of the absolute value for these SPs. In this report, we have compared the results of our VUV SE against the results obtained by using dichroic dye film type polarizers in the visible region (300 ~ 500 nm) for the SPs of BL7B output beam to further confirm the correctness of the absolute SPs based on our SE.

Figure 1 shows schematic layout of our VUV SE with Au mirror as a standard sample. Measurement system using the VIS polarizer is shown in Fig. 2. In Fig. 2, since the polarizer set at the sample position instead of a Au mirror is a transmission type, optical conditions are the same between two methods. Figure 3 shows SPs of BL7B output beam as a function of wavelength obtained by our VUV SE (solid circles) and polarizers (open circles). It is noted that S_3/S_0 and unpolarized components cannot be distinguished in the experiment by using the polarizer. As expected from both the characteristics of SR and the optical configuration of the BL7B, the results of both experimental methods show that S_1/S_0 values are close to 1 and both S_2/S_0 and S_3/S_0 have small values. The agreements between the two methods for both S_2/S_0 and S_1/S_0 in all wavelength region validates our SE.

[1] W. Budde and R. Dittmann, PTB-Mitt. **83** (1973) 1.
[2] T. Saito, M. Yuri and H. Onuki, Rev. Sci. Instrum. **66** (1995) 1570.
[3] T. Saito, K. Ozaki, K. Fukui, H. Iwai, K. Yamamoto, H. Miyake and K. Hiramatsu, Thin Solid Films **571** (2014) 517.

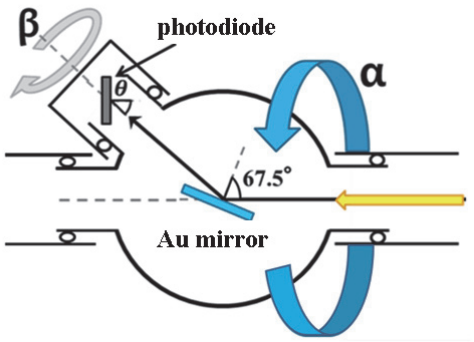

Fig. 1. Schematic layout of VUV SE.

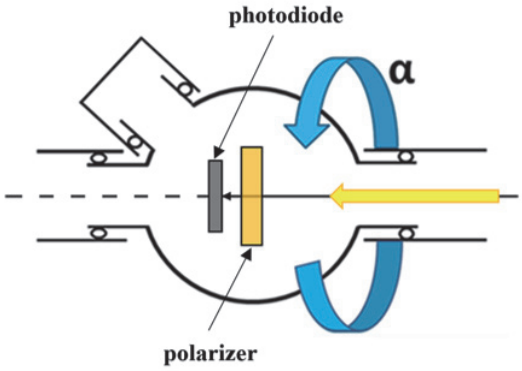

Fig. 2. Schematic layout of Stokes parameters measurement system using a polarizer.

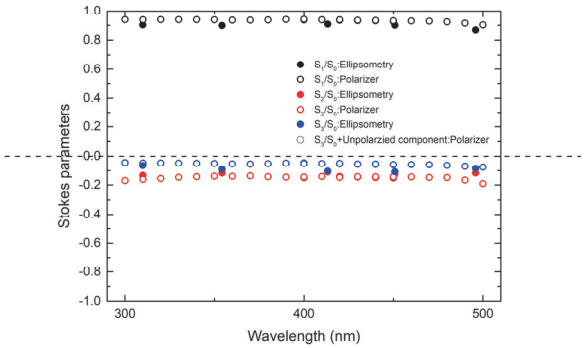

Fig. 3. Stokes parameters of BL7B.

UVSOR User 1